Bioorganic & Medicinal Chemistry Letters 24 (2014) 5818–5823

Contents lists available at ScienceDirect

Bioorganic & Medicinal Chemistry Letters

journal homepage: www.elsevier.com/locate/bmcl

Design, synthesis and structure–activity relationships of a novel class of sulfonylpyridine inhibitors of Interleukin-2 inducible T-cell kinase (ITK)

Giancarlo Trani [a,*], John J. Barker [a], Steven M. Bromidge [a], Frederick A. Brookfield [a], Jason D. Burch [b], Yuan Chen [b], Charles Eigenbrot [b], Alexander Heifetz [a], M. Hicham A. Ismaili [b], Adam Johnson [b], Thomas M. Krülle [a], Colin H. MacKinnon [a], Rosemary Maghames [a], Paul A. McEwan [a], Christian A. G. N. Montalbetti [a], Daniel F. Ortwine [b], Yolanda Pérez-Fuertes [a], Darshan G. Vaidya [a], Xiaolu Wang [c], Ali A. Zarrin [b], Zhonghua Pei [b]

[a] Discovery Chemistry, Evotec UK Ltd, 114 Innovation Drive, Milton Park, Abingdon, OX14 4RZ, UK
[b] Discovery Chemistry, Genentech, Inc., 1 DNA Way, South San Francisco, CA 94080, USA
[c] Discovery Biology, Evotec AG, Manfred Eigen Campus, Essener Bogen 7, D-22419 Hamburg, Germany

ARTICLE INFO

Article history:
Received 29 August 2014
Revised 30 September 2014
Accepted 1 October 2014
Available online 12 October 2014

Keywords:
ITK inhibitor
T-cell receptor
Sulfonylpyridine

ABSTRACT

Starting from benzylpyrimidine **2**, molecular modeling and X-ray crystallography were used to design highly potent inhibitors of Interleukin-2 inducible T-cell kinase (ITK). Sulfonylpyridine **4i** showed sub-nanomolar affinity against ITK, was selective versus Lck and its activity in the Jurkat cell-based assay was greatly improved over **2**.

Interleukin-2 inducible T cell kinase (ITK, also known as Emt or Tsk), is a member of the Tec family of tyrosine kinases and is mainly expressed in T cells, mast cells and natural killer cells. In T cells, ITK is activated after T-cell receptor (TCR) stimulation leading to phosphorylation of phospholipase C-γ1 (PLC-γ1), calcium mobilization, IL-2 production, and cell proliferation and differentiation.[1,2] Deletion of ITK in mice results in reduced production of Th2 cytokines such as IL-4, IL-5 and IL-13.[3] ITK has been shown to play an important role in the development of T-cell dependent late phase responses of allergic asthma. In studies with $ITK^{-/-}$ mice, the immunological symptoms of allergic asthma are attenuated and lung inflammation, eosinophil infiltration and mucus production are drastically reduced in response to challenge with the allergen ovalbumin.[4] Similar results were reported with a selective ITK inhibitor[5] indicating a potential role of ITK kinase activity in inflammatory processes. Therefore, selective inhibition of ITK could represent an attractive approach for the treatment of T-cell mediated diseases.

The initial optimization work carried out on an HTS hit from the Genentech compound collection (unpublished data) led to the identification of benzylpyrimidine **2** (Fig. 1), a compound which combines the features of the initial Genentech HTS hit **1a** and another ITK inhibitor **1b** previously published by researchers at GSK.[6] Compound **2** had improved kinetic aqueous solubility (70 μM) compared to **1b** (⩽1 μM) and showed high inhibitory activity against ITK (K_i = 53 nM);[7] however, when it was tested against lymphocyte-specific kinase (Lck), another T-cell tyrosine kinase which operates upstream of ITK in the TCR cascade, it showed a complete lack of selectivity (3.5-fold) and its activity in a Jurkat cell-based assay,[8] as measured by inhibition of phosphorylation of PLC-γ1, was sub-optimal (IC_{50} = 2.6 μM). Here we describe the further optimization of compound **2**, which led to the identification of a novel series of sulfonylpyridines as selective ITK inhibitors with improved activity in the Jurkat cell-based assay compared to **2**.

In silico modeling of **2** in the ITK kinase domain gave rise to the binding hypothesis which is summarized in Figure 2. The aminopyrazole portion forms three hydrogen bonds with Met438 and Glu436 of the hinge region and the benzene ring of the substituent at the 6-position of the pyrimidine is involved in an edge–face

* Corresponding author.
E-mail address: Giancarlo.Trani@evotec.com (G. Trani).

http://dx.doi.org/10.1016/j.bmcl.2014.10.020
0960-894X/

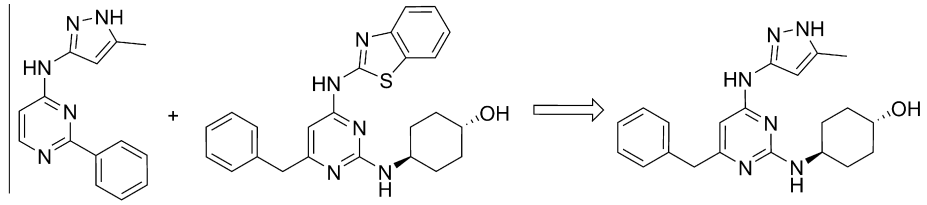

1a ITK K_i = 3000 nM

1b ITK K_i = 4 nM

2 ITK K_i = 53 nM, Lck/ITK = 3.5, p-PLCγ1 IC_{50} = 2600 nM

Figure 1. Hit to lead studies.

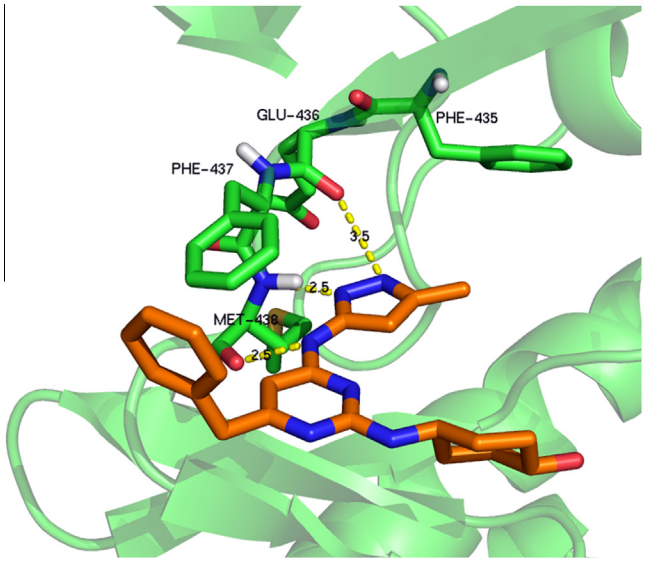

Figure 2. In silico modeling of compound **2** in the ITK kinase domain.

interaction with Phe437, which is proposed to account for the majority of the potency boost over the initial HTS hit **1a**. The same interactions were also observed in the X-ray crystal structures of two other ITK inhibitors (indazole and benzothiazole) discovered at Genentech.[9]

We initially sought to replace the benzylic carbon with alternative linkers in order to modulate the angles between the pyrimidine core and the phenyl ring, in an attempt to maximize the interaction with Phe437 and selectivity against Lck, which contains a tyrosine (Tyr318) in place of Phe437 in ITK. Sulfonylpyrimidine **3** (Table 1) showed the highest affinity amongst the linkers explored (ether, thioether, sulfone), with a K_i against ITK of 177 nM. Although less active than **2**, we envisioned that the loss in affinity could be the result of an electronic repulsion between the oxygens of the sulfonyl linker and the lone pair of the proximal nitrogen of the pyrimidine core, disfavoring the phenyl ring from adopting the desired bioactive conformation required for interaction with Phe437. This observation was supported by a conformational analysis[10] performed on the model system 4-methanesulfonyl-pyrimidine, as shown in Figure 3A. The minimization of steric interactions and electronic repulsions suggested an energy minimum at a dihedral angle of 120°, while the optimal bioactive conformation as predicted by the docking (Fig. 2) was circa 4 kcal/mol higher in energy, at an angle of about 60°. A similar analysis performed on

Table 1
Data for sulfonylpyrimidine **3** and sulfonylpyridine **4a**

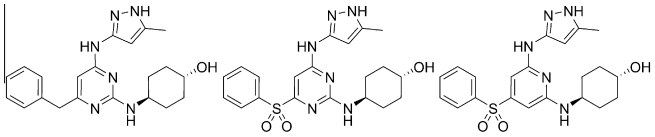

2 **3** **4a**

Compound	ITK K_i (nM)	Fold selectivity over Lck	p-PLCγ1 IC_{50} (nM)	Kin. Sol. (μM)
2	53	3.5	2600	70
3	177	1.5	—	39
4a	4	34	540	32

4-methanesulfonyl-pyridine (Fig. 3B) which lacks the nitrogen lone pair *ortho* to the sulfonyl linker revealed an energy minimum at 90°. In this system, the putative bioactive conformation was much closer to the minimum and only 1 kcal/mol higher in energy, thus decreasing the enthalpic penalty of binding. Based on this hypothesis we prepared the sulfonylpyridine **4a** and we were pleased to see that the experimental results reflected what was predicted in the torsional scan. Compound **4a** was not only very potent (ITK K_i = 4 nM), showing 44-fold increase in potency over **3** and 13-fold over **2**, but it also showed improved selectivity against Lck (34-fold) compared to **2** (3.5-fold).

In order to explore whether the binding energy of **4a** could be further improved, we prepared a range of heterocycles (Table 2).

Compound **5** where the pyrazole was replaced by an imidazole displayed a 3-fold drop in potency and loss of Lck selectivity. Thiazole **6a** showed sub-nanomolar affinity for ITK, (K_i = 0.27 nM); however, its affinity for Lck was also in the low nanomolar range. We believe that the different shape of the thiazole which allows for more effective hydrogen bond interactions with the hinge sequence, the restricted rotation of the thiazole ring across the NH—C bond and a higher desolvation penalty associated to the pyrazole compared to the thiazole, all contributed to the 15-fold increase in potency observed for compound **6a** over **4a**.

Benzothiazole **6b** had similar potency to pyrazole **4a** but showed >100-fold selectivity against Lck. Although compounds **6a** and **6b** were respectively more active and selective than **4a**, they were also more lipophilic, and in the case of **6b** contained an additional aromatic ring. This led to poor kinetic solubility which was reflected in a higher solubility forecast index (SFI),[11] a simple metric which has been used as a tool to predict solubility via the sum of $c\mathrm{Log}D_{7.4}$ and aromatic ring count.

Given its favorable potency and selectivity profile, we further explored the SAR of the more soluble pyrazole **4a** (Table 3). We

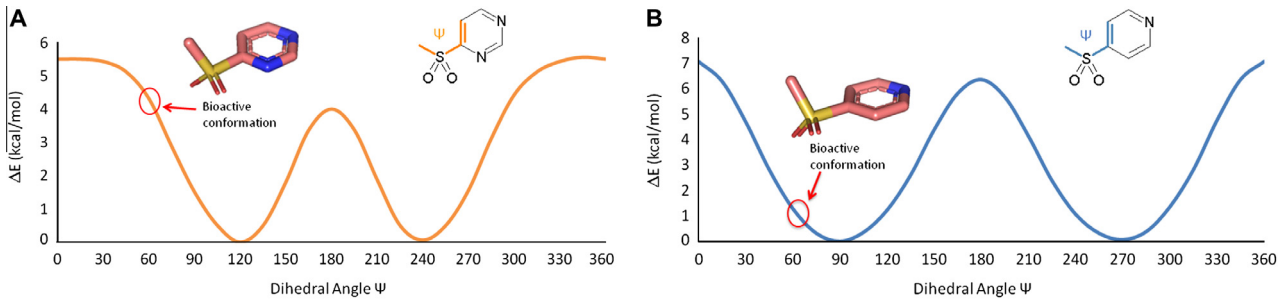

Figure 3. Dihedral torsional scan performed on 4-methanesulfonyl-pyrimidine (A) and on 4-methanesulfonyl-pyridine (B).

Table 2
Hinge binder exploration

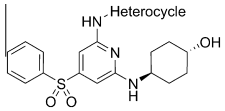

Compound	Heterocycle	ITK K_i (nM)	Fold selectivity over Lck	Kin. Sol. (μM)	SFI
4a		4	34	32	7.7
5		14	3	6	6.7
6a		0.27	11	⩽1	8.1
6b		8	106	⩽1	10

Table 3
SAR around the pyrazole hinge binder

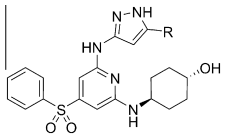

Compound	R	ITK K_i (nM)	Fold selectivity over Lck	Kin. Sol. (μM)	SFI
4a	Me	4	34	32	7.7
4b		2.3	9	⩽1	10.3
4c		5.3	11	⩽1	10.1
4d	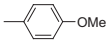	1.2	10	⩽1	10.4
4e		1.8	16	⩽1	10.5
4f	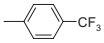	20	n.d.	⩽1	11.3
4g	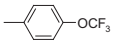	61	n.d.	⩽1	11.6
4h		1.6	39	8.8	8.4
4i		0.17	182	⩽1	8.8
4j		0.38	45	⩽1	9.3

reasoned that ITK activity and selectivity against Lck could be further improved by exploiting the difference in the gatekeeper residue between the two kinases (Phe435 in ITK, Thr316 in Lck).

A phenyl group directly attached to the pyrazole ring (compound **4b**) showed similar potency to **4a**. The activity was minimally affected by the introduction of small substituents on the phenyl ring, as shown by compounds **4c**–**g**, with *para*-substitution (**4d**) preferred over *meta*- (**4c**). However, larger, lipophilic substituents led to a drop in potency (**4f** and **4g**), presumably due to a clash with the gatekeeper residue.

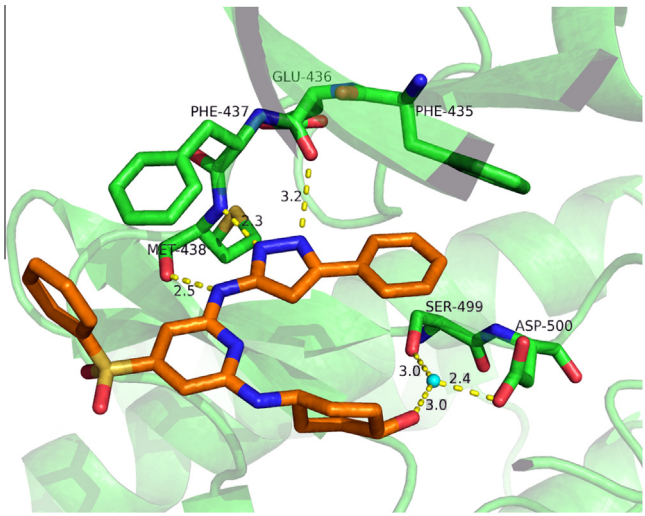

Figure 4. X-ray structure of **4b** in the ITK kinase domain (resolution 2.6 Å, PDB code 4QD6). Only selected residues of ITK are shown for clarity. Protein–ligand hydrogen bonds are indicated by the dashed lines in yellow.

In order to validate the binding hypothesis, we determined the crystal structure of compound **4b** bound in the ITK active site. The structure, solved at 2.6 Å resolution, confirmed many of the features predicted by the in silico model (Fig. 4).[12] The aminopyrazole moiety forms three hydrogen bonds with the hinge sequence (Met438 and Glu436). The pyridine core is positioned in the same plane of the aminopyrazole, sandwiched in a narrow lipophilic cleft, and the sulfone linker positions the phenyl ring at a dihedral angle of 60° from the pyridine core, giving a close edge–face interaction with Phe437. The crystal structure also revealed that the hydroxyl of the cyclohexanol group forms a hydrogen bond to a water molecule which is further stabilized by hydrogen bonds with Ser499 and Asp500.

The phenyl ring at the 5-position of the pyrazole is involved in an edge–face interaction with the gatekeeper Phe435. Unfortunately, this only slightly improved ITK activity over **4a** (compounds **4b**–**e**), and was also associated with an equal increase in affinity for Lck, presumably due to a π–OH interaction with the Thr316 gatekeeper in Lck. Furthermore, the presence of the extra aromatic ring led to a deterioration in aqueous solubility of **4b**–**g** relative to **4a**, and therefore we investigated the replacement of the phenyl ring with alkyl groups.

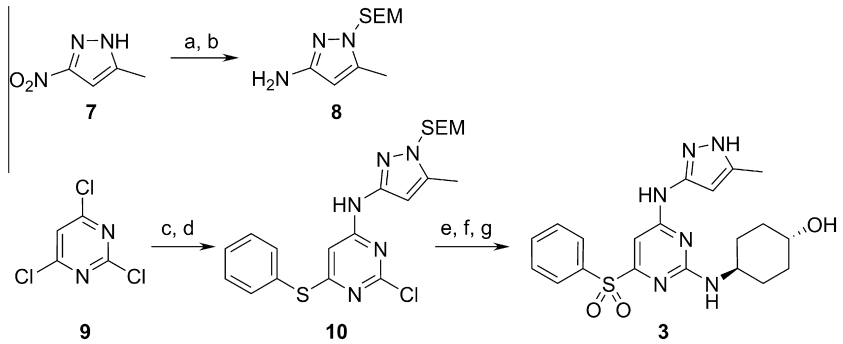

Scheme 1. Reagents and conditions: (a) SEM-Cl, DIPEA, CH_2Cl_2, RT, 20 h; (b) H_2, Pd/C, ethanol, RT, 20 h, 41% over two steps; (c) Thiophenol, NaOH, acetone/water (1:1), RT, 1 h, 80%; (d) **8**, DIPEA, ethanol, 85 °C, 37 h, 52%; (e) *trans*-4-aminocyclohexanol, 2-propanol, 150 °C in microwave, 4 h, 90%; (f) *m*CPBA, CH_2Cl_2, RT, 45 min, 47%; (g) HCl (4 M in 1,4-dioxane), RT, 20 h, 37%.

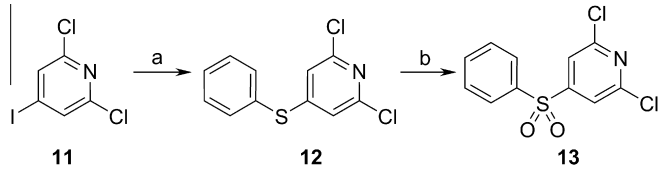

Scheme 2. Reagents and conditions: (a) thiophenol, $Pd_2(dba)_3$, xantphos, DIPEA, 1,4-dioxane, 110 °C, 1.5 h, 77%; (b) *m*CPBA, CH_2Cl_2, RT, 4 h, 90%.

Gratifyingly, we found that aliphatic substituents (**4h–j**) were well tolerated and in general led to improved ITK affinity and increased Lck selectivity. Cyclobutane **4h** had ITK K_i = 1.6 nM and was 39-fold selective versus Lck. Increasing the size to cyclopentane **4i** led to a 9.5-fold increase in potency (ITK K_i = 0.17 nM) compared to **4h** and selectivity versus Lck was also improved (182-fold). This boost in potency and selectivity is likely due to the ability of the cyclopentane ring to establish more effective lipophilic interactions with Phe435 in ITK than with Thr316 in Lck. When the size of the alkyl substituent was increased further (cyclohexane **4j**), ITK activity started to plateau and selectivity to decrease. Although alkyl pyrazoles **4h–j** have a lower SFI compared to the aryl analogs **4b–g** due to the former having one less aromatic ring, the increasing size of the alkyl groups necessary for better activity and selectivity, also contributed to a higher Log*D*, resulting in no improvement of aqueous solubility compared to the aryl analogs, thus suggesting that in order to obtain compounds with measurable solubility a hard cut-off of SFI = 7 should be observed in this series.

Compound **4i** (Table 3) had the best ITK activity and selectivity versus Lck and it was selected for further profiling. It showed moderate to high clearance in human liver microsomes (16 mL/min/kg), no P450 inhibition below 8 μM (against 2C9, 2C19, 2D6 and 3A4) and moderate permeability as measured in the MDR1/MDCK assay (P_{app} apical to basolateral (AB) = 2.5×10^{-6} cm/s, P_{app} basolateral to apical (BA) = 12×10^{-6} cm/s, BA/AB = 4.8). **4i** also inhibited PLC-γ1 phosphorylation in Jurkat cells with an IC_{50} = 180 nM, a 15-fold improvement over **2**. Invitrogen kinase selectivity profiling of **4i** at 0.1 μM (40 kinases) resulted in only 3 kinases showing greater than 70% inhibition (CDK2, Flt3 and MuSK).

Compounds **3**, **4a–j**, **5** and **6a–b** were prepared as described in Schemes 1–4. Sulfonylpyrimidine **3** was prepared in five steps starting from 2,4,6-trichloropyrimidine **9** (Scheme 1). Reaction with thiophenoxide ion at room temperature followed by a second nucleophilic displacement with SEM-protected aminopyrazole **8** afforded the 2-chloropyrimidine **10**. A third nucleophilic substitution with *trans*-4-aminocyclohexanol, followed by oxidation of the thioether to the corresponding sulfone and final deprotection of the pyrazole with HCl at room temperature afforded the desired pyrimidine sulfone **3**. Aminopyrazole **8** (Scheme 1) was obtained

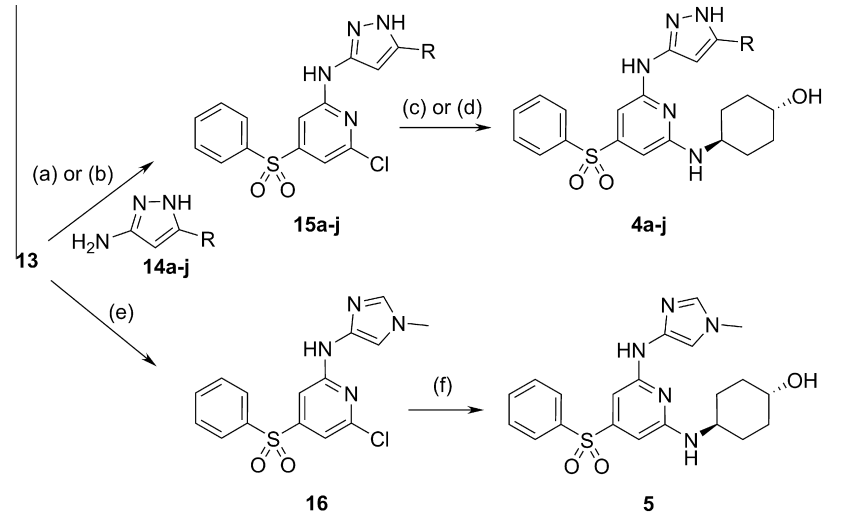

Scheme 3. Reagents and conditions: (a) DIPEA, DMSO, 100–110 °C, up to 36 h; (b) DIPEA, DMSO, 150–165 °C in microwave, up to 6 h, 23–62%; (c) *trans*-4-aminocyclohexanol, DIPEA, DMSO, 120 °C, up to 20 h; (d) *trans*-4-aminocyclohexanol, DIPEA, DMSO, 170 °C in microwave, up to 2 h, 10–54%; (e) 1-methyl-4-aminoimidazole, DIPEA, DMSO, 120 °C, 2 h, 24%; (f) *trans*-4-aminocyclohexanol, DIPEA, DMSO, 120 °C, 20 h, 31%.

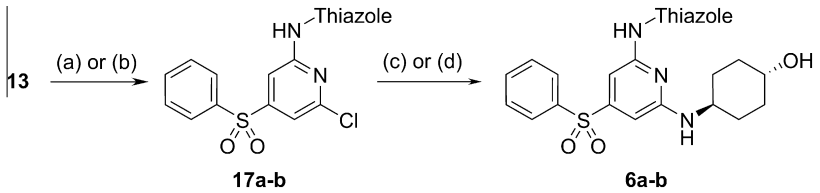

Scheme 4. Reagents and conditions: (a) 2-amino-5-methylthiazole, $Pd_2(dba)_3$, xantphos, Na_2CO_3, 1,4-dioxane, 100 °C, 2 h, 52%; (b) 2-aminobenzothiazole, $Pd_2(dba)_3$, xantphos, Na_2CO_3, 1,4-dioxane, 150 °C in microwave, 45 min, 40%; (c) **17a**, *trans*-4-aminocyclohexanol, $Pd_2(dba)_3$, BINAP, NaO^tBu, DME, 85 °C, 20 h, 35%; (d) **17b**, *trans*-4-aminocyclohexanol, DMSO, 150 °C in microwave, 1.5 h, 19%.

by reaction of 3-methyl-5-nitropyrazole **7** with (2-chloromethoxy-ethyl)-trimethyl-silane followed by catalytic hydrogenation over palladium on charcoal and final separation of the regioisomers by chromatography.[13]

The building block 4-benzenesulfonyl-2,6-dichloropyridine **13** (Scheme 2) was prepared in two steps from commercially available 2,6-dichloro-4-iodopyridine **11** by palladium catalyzed cross-coupling with thiophenol, followed by oxidation of thioether **12** with *meta*-chloroperbenzoic acid.

Compounds **4a–j** were synthesized from **13** in two successive nucleophilic displacements, initially with the desired 3-aminopyrazole followed by *trans*-4-aminocyclohexanol (Scheme 3). Aminopyrazoles **14a–f** and **14h–j** were all commercially available, while **14g** was prepared by cyclization of the corresponding 3-oxo-3-(4-trifluoromethoxy-phenyl)-propionitrile with hydrazine according to the literature procedure.[14] Compound **5** (Scheme 3) was prepared in an analogous manner to **4a–j**, using 1-methyl-4-aminoimidazole in the first nucleophilic displacement.

Attempts at installing the aminothiazole moiety by nucleophilic substitution on dichloropyridine **13** in the presence of mild organic bases were unsuccessful due to the low reactivity of the aminothiazole. Increasing the nucleophilicity by formation of the anion with sodium hydride led to the preferential displacement of the sulfone group at the 4-position. This issue was overcome by performing a palladium catalyzed amination to afford intermediates **17a–b** (Scheme 4). The *trans*-4-aminocyclohexanol was then installed either by nucleophilic displacement in DMSO or by palladium catalyzed cross-coupling to afford compounds **6a–b**.

In conclusion, starting from the non selective benzylpyrimidine **2**, by judicious choice of the linker and optimization of small molecule conformations we have identified a new class of highly potent and selective ITK inhibitors, as exemplified by compound **4i**. The intrinsic potency, selectivity versus Lck and cellular activity were all improved over the lead compound; however, further improvements in physicochemical properties and in particular solubility are required.

References and notes

1. Schaeffer, E. M.; Debnath, J.; Yap, G.; McVicar, D.; Liao, X. C.; Littman, D. R.; Sher, A.; Varmus, H. E.; Lenardo, M. J.; Schwartzberg, P. L. *Science* **1999**, *284*, 638.
2. Fowell, D. J.; Shinkai, K.; Liao, X. C.; Beebe, A. M.; Coffman, R. L.; Littman, D. R.; Locksley, R. M. *Immunity* **1999**, *11*, 399.
3. Miller, A. T.; Wilcox, H. M.; Lai, Z.; Berg, L. J. *Immunity* **2004**, *21*, 67.
4. Mueller, C.; August, A. *J. Immunol.* **2003**, *170*, 5056.
5. Lin, T. A.; McIntyre, K. W.; Das, J.; Liu, C.; O'Day, K. D.; Penhallow, B.; Hung, C. Y.; Whitney, G. S.; Shuster, D. J.; Yang, X.; Townsend, R.; Postelnek, J.; Spergel, S. H.; Lin, J.; Moquin, R. V.; Furch, J. A.; Kamath, A. V.; Zhang, H.; Marathe, P. H.; Perez-Villar, J. J.; Doweyko, A.; Killar, L.; Dodd, J. H.; Barrish, J. C.; Wityak, J.; Kanner, S. B. *Biochemistry* **2004**, *43*, 11056.
6. Alder, C. M.; Baldwin, I. R.; Barton, N. P.; Campbell, A. J.; Champigny, A. C.; Harling, J. D.; Maxwell, A. C.; Simpson, J. K.; Smith, I. E. D.; Tame, C. J.; Wilson, C.; Woolven, J. M. WO2010/106016 A1; Alder, C. M.; Ambler, M.; Campbell, A. J.; Champigny, A. C.; Deakin, A. M.; Harling, J. D.; Harris, C. A.; Longstaff, T.; Lynn, S.; Maxwell, A. C.; Mooney, C. J.; Scullion, C.; Singh, O. M. P.; Smith, I. E. D.; Somers, D. O.; Tame, C. J.; Wayne, G.; Wilson, C.; Woolven, J. M. *ACS Med. Chem. Lett.* **2013**, *4*, 948.
7. GST-ITK and LCK-HIS full length enzymes were from Invitrogen (PV3875 and P3043, respectively) and substrate was BLK peptide (Ac-EFPIYDFLPAKKK-NH_2). Reactions were carried out in a final volume of 51 µl with 50 mM HEPES buffer (pH 7.2), 15 mM $MgCl_2$, 2 mM DTT, 0.015% Brij-35, 1 nM ITK or 0.5 nM LCK, 2 µM substrate, 20 µM ATP, and test article in a final concentration of 2% DMSO. After 35 min incubation at RT, reactions were stopped upon addition of 10 µl of 30% TCA. Samples were centrifuged (4350 rpm, 4 °C, 5 min) and subjected to LC/MS analysis on a Waters Acquity UPLC/TQD system equipped with a Waters Acquity UPLC BEH C18 (2.1 × 50 mm) 1.7 µm column (injection volume: 5 µl, column temperature: 60 °C, flow rate: 1 ml/min, solvent A: 0.1% formic acid in LC/MS grade water, solvent B: 0.1% formic acid in LC/MS grade ACN). Analytes were separated by applying a gradient from 15% to 32% solvent B within 0.7 min and detected in positive mode ESI-MS/MS by MRM (multiple reaction monitoring) of transitions 819.8/84.8 (BLK substrate) and 859.0/84.8 as well as 859.0/120.7 (phosphorylated BLK product). K_i values were determined using the Morrison tight-binding equation (William, J. W.; Morrison, J. F. *Methods Enzymol.* **1979**, *63*, 437.), modified to account for an ATP-competitive mechanism of inhibition and for the concentration of active kinase used.
8. Jurkat T-cells (400 K cells/well) were suspended in assay buffer (D-PBS + 0.1% glucose + 0.22 µM sodium pyruvate), seeded in 96-well plate, treated with compounds for 30 min, and stimulated with anti-CD3 Dynabeads (Invitrogen, 400 K beads/well) for 2 min at 37 °C. The cells were pelleted by brief spinning, and after aspirating off media, 30 µl of 1× lysis buffer (Cell Signaling Technology) was added to each well, and plate was incubated at 4 °C for 30 min while shaking. After beads were quickly spinned down, 25 µl of lysate from each well were transferred to capture antibody (mouse monoclonal antibody to human PLC γ1, from Abcom) coated MSD goat anti-mouse 96-well plate (MesoScale Discovery), and incubated at 4 °C overnight with shaking. After 4× wash with 150 µl MSD Tris buffer (50 mM Tris–HCl, pH 7.5, 150 mM NaCl, 0.02% Tween-20), 25 µL of detection antibodies (1:2000 dilution mixture of rabbit anti-pPLCγ1, from Cell Signaling Technology and goat anti-rabbit SULFO-Tag from MesoScale Discovery) to each well, and incubated for 2 h at room temperature. After washing of the plate with 4 × 150 µL of MSD Tris buffer, 150 µl of 1× MSD read buffer T was added to each well, and the plate was read out on SECTOR Imager 6000 (MesoScale Discovery).
9. (a) Pastor, R. M.; Burch, J. D.; Magnuson, S.; Ortwine, D. F.; Chen, Y.; De La Torre, K.; Ding, X.; Eigenbrot, C.; Johnson, A.; Liimatta, M.; Liu, Y.; Shia, S.; Wang, X.; Wu, L. C.; Pei, Z. *Bioorg. Med. Chem. Lett.* **2014**, *24*, 2448; (b) Burch, J. D.; Lau, K.; Barker, J. J.; Brookfield, F.; Chen, Y.; Chen, Y.; Eigenbrot, C.; Ellebrandt, C.; Ismaili, M. H. A.; Johnson, A.; Kordt, D.; MacKinnon, C. H.; McEwan, P. A.; Ortwine, D. F.; Stein, D. B.; Wang, X.; Winkler, D.; Yuen, P.-W.; Zhang, Y.; Zarrin, A. A.; Pei, Z. *J. Med. Chem.* **2014**, *57*, 5714; (c) MacKinnon, C. H.; Lau, K.; Burch, J. D.; Chen, Y.; Dines, J.; Ding, X.; Eigenbrot, C.; Heifetz, A.; Jaochico, A.; Johnson, A.; Kraemer, J.; Kruger, S.; Krülle, T. M.; Liimatta, M.; Ly, J.; Maghames, R.; Montalbetti, C. A. G. N.; Ortwine, D. F.; Pérez-Fuertes, Y.; Shia, S.; Stein, D. B.; Trani, G.; Vaidya, D. G.; Wang, X.; Bromidge, S. M.; Wu, L. C.; Pei, Z. *Bioorg. Med. Chem. Lett.* **2013**, *23*, 6331.
10. The conformational analysis was performed using torsional sampling every 15° around the S—Heterocycle bond. The energy of each conformer was calculated by quantum mechanical methods at MP2/3-21G* level of theory with polarisable continuum model (PCM) of water using GAMESS.
For details about GAMESS see 'Advances in electronic structure theory: GAMESS a decade later' Gordon, M. S.; Schmidt, M. W. In *Theory and Applications of Computational Chemistry: The First Forty Years*, Dykstra, C. E.; Frenking, G.; Kim, K. S.; Scuseria, G. E., Eds.; Elsevier: Amsterdam, 2005; pp 1167–1189.
11. Hill, A. P.; Young, R. J. *Drug Discovery Today* **2010**, *15*, 648.
12. The crystal structure of **4b** in complex with ITK was determined from crystals of ITK soaked with 2 mM compound for 4 days. Crystals of ITK (residues 357–620) were prepared from recombinant protein prepared from baculovirus infected SF9 cells. The protein was incubated on ice in the presence of 4 mM AMP-PNP and 2 mM magnesium chloride for 2 h prior to crystal trials. Crystallisation drops were set at 1:1 ratio of protein and precipitant consisting of 0.2 M sodium nitrate, 0.1 M bis tris propane pH 8.5 and 20% PEG 3350. Plate shaped crystals typically appear within a week at 4 °C and require multiple rounds of macro-seeding to achieve sufficiently large crystals.

Diffraction data were collected at beamline IO4-1 of Diamond Light Source (Didcot, Oxfordshire, UK) at a wavelength of 0.917 Å. The structure was solved by molecular replacement and refined using the program REFMAC and rebuilding in the program COOT.
For details about REFMAC see 'Refinement of Macromolecular Structures by the Maximum-Likelihood Method' Murshudov, G. N.; Vagin, A. A.; Dodson, E. J. *Acta Crystallogr*. **1997**, *D53*, 240.
For details about COOT see: 'Features and Development of Coot' Emsley, P.; Lohkamp, B.; Scott, W.; Cowtan, K. *Acta Crystallogr*. **2010**, *D66*, 486.

13. The more polar, slow running regioisomer, was tentatively assigned as structure **8** (Scheme 1) and was carried forward to the next stage.
14. Haydar, S. N.; Bothmann, H.; Ghiron, C.; Maccari, L.; Micco, I.; Nencini, A.; Zanaletti, R. WO 2010/009290 A1; *Chem. Abstr*. **2010**, *152*, 192109.